

RESEARCH

Open Access



# New insights on collagen structural organization and spatial distribution around dental implants: a comparison between machined and laser-treated surfaces

Alessia Belloni<sup>1†</sup>, Giulio Argentieri<sup>2†</sup>, Giulia Orilisi<sup>3</sup>, Valentina Notarstefano<sup>1</sup>, Elisabetta Giorgini<sup>1</sup>, Gianmaria D'Addazio<sup>2</sup>, Giovanna Orsini<sup>3\*</sup> , Sergio Caputi<sup>2</sup> and Bruna Sinjari<sup>2</sup>

## Abstract

**Background** One of the main factors for the osseointegration of dental implants is the development of an adequate soft tissue barrier, mainly composed by collagen, which protects the implant from bacterial development. The structural features of the peri-implant collagen are influenced by the implant components and, in particular, by the type of the surface. In the clinical practice, healing abutments are characterized by smooth surfaces, named machined. Recently, a new laser technique, Synthegra, has been developed to obtain a topography-controlled surface with micrometric regular pores that seems reducing the risk of peri-implantitis. Based on this background, this study aims investigating the structural organization and spatial distribution of collagen surrounding healing abutments characterized by laser-treated and machined surfaces.

**Methods** Gingiva portions surrounding custom-made healing abutments (HA), characterized by alternated laser-treated and machined surfaces, were collected and analyzed by combining Fourier Transform InfraRed Imaging (FTIRI) spectroscopy, a non-invasive and high-resolution bidimensional analytical technique, with histological and multivariate analyses.

**Results** Masson's trichrome staining, specific for collagen, highlighted a massive presence of collagen in all the analyzed samples, evidencing a surface-related spatial distribution. The nature of collagen, investigated by the FTIRI spectroscopy, appeared more abundant close to the laser-treated surface, with a perpendicular disposition of the bundles respect to the HA; conversely, a parallel distribution was observed around the machined surface. A different secondary structure was also found, with a higher amount of triple helices and a lower quantity of random coils in collagen close to the laser treated surfaces.

**Conclusions** FTIRI spectroscopy demonstrates that the use of a laser treated transmucosal surface can improve the morphological organization of the peri-implant collagen, which presents a distribution more similar to that of natural teeth.

<sup>†</sup>Alessia Belloni and Giulio Argentieri equally contributed to the study.

\*Correspondence:

Giovanna Orsini

g.orsini@staff.univpm.it

Full list of author information is available at the end of the article



*Trial registration:* This trial is registered with ClinicalTrials.gov Identifier: (Registration Number: NCT05754970). Registered 06/03/2023, retrospectively registered, <https://clinicaltrials.gov/show/NCT05754970>.

**Keywords** Dental implants, Collagen, Implant surface, Synthebra, Healing abutments, Fourier Transform InfraRed Imaging spectroscopy, Transmucosal surface

## Background

Modern literature agrees that implantology is a highly reliable and predictable procedure, with a survival rate of about 90% in a medium to long-term follow-up period [1]. However, dental implants are not completely free from biological and mechanical complications [2]. Biological failure has been defined as the inadequacy of the host tissue to establish or maintain osseointegration [3]. It can be classified into early and late failure. Early failure can occur in the first few weeks or maximum a few months after implant placement. It may depend on the intrinsic properties of the host tissue; in general, it is caused by a biological agent which hinders surgical wound healing and, hence, prevents the achievement of the osseointegration [4]. Late failure refers to an implant that has lost the achieved osseointegration due to the onset of peri-implantitis [5], an inflammatory pathological condition that affects the peri-implant soft and hard tissues leading to the progressive loss of supporting bone and thus to implant failure [6]. Peri-implant mucositis develops from healthy peri-implant mucosa as a result of bacterial biofilm accumulation around osseointegrated dental implants [7]. Peri-implant disease shows an etiopathogenetic mechanism and its risk factors are very similar to periodontal disease [8–10]. Studies in dogs have shown that the inflammatory infiltrate in peri-implant tissues is greater than that which develops in periodontal tissues [5, 11, 12]. The inflammation at the level of the implants arises because there are no supracrestal fibers to stem the disease as in periodontitis. In addition, unlike periodontitis, in peri-implantitis inflammation also occurs at the bone level (osteitis), again due to the lack of these supracrestal fibers, which act as a barrier [5].

Collagen stands as the predominant fibrous protein in the extracellular matrix in all mammalian connective tissues; it forms an essential framework used by fibroblasts as scaffolding to "crawl" along [13, 14]. It serves as the primary structural component, crucial for upholding tissue mechanical properties, offering tensile strength, and overseeing vital processes like cell adhesion and tissue development [15]. Structurally, collagen presents a triple-stranded helical arrangement, comprising three left-handed  $\alpha$ -chains coiled around each other to form a right-handed super-helix [16, 17].

As collagen plays a pivotal role in the structure and function of the ECM, any irregularities in its composition or organization inevitably lead to altered tissue characteristics. One of the main differences between the gingival tissues surrounding a natural tooth and a dental implant is the collagen fiber orientation around the collar of the device just below the gingival surface. In a natural tooth, dentogingival collagen fibers are inserted into the cementum and the bone, and oriented perpendicular or oblique to the tooth surface [18, 19]. In contrast, around a dental implant they are mainly parallel to the implant surface [20, 21].

The adhesion of the soft tissue to the implant, called transmucosal attachment, acts as a seal which prevents damages to osseointegration processes, avoiding the formation and attachment of microorganisms to the bone tissue [22]. It represents the result of a surgical wound healing, unlike the soft tissues around the tooth which develops at the same time as the periodontium [23, 24]. Many studies have shown how the structural features of the implant, such as the surface chemistry and topography, the macro- and micro-designs of abutments [25], the wettability [26] and the presence of biologically active proteins [27–30], can influence the adhesion of the junction epithelium and of the connective tissue to the abutment surface [31].

The literature agrees that surface roughness can influence cell adhesion [32]. Among all, laser treatment, a procedure which causes an increase of the surface roughness, has been shown to be very beneficial both for reducing bacterial contamination [33] and maintaining the mechanical characteristics [34]. In this light, the Synthebra technique, a recently developed procedure based on a new generation of laser technology, has shown promising results [35, 36]. The laser, moving along the implant surface, removes titanium by sublimation and creates thousands of micrometric pores with regular distribution and equal in shape and size: micropores have a diameter of 5 microns, an interpore distance of 15 microns and a depth of 5 microns. The result is a clean, topography-controlled surface that induces excellent osseointegration and significantly reduction of bacterial adhesion, resulting in a lower risk of peri-implantitis [36].

Fourier Transform Infrared Imaging (FTIRI) spectroscopy is a well assessed and label-free tool for studying non-homogeneous biological samples such as tissues and

cells [37, 38]. In fact, the coupling between infrared spectroscopy and visible microscopy and the development of array detectors able to reach a spatial resolution down to a few microns, let obtain high-resolution IR images which simultaneously provide reliable information on the biomolecular composition and structural organization of several macromolecules, including proteins and collagen [17, 39]. Recently, FTIRI has been successfully applied for exploring the structural organization of collagen in soft and hard tissues and interesting results have been obtained [37, 38].

In this light, in the present study, we propose a multidisciplinary approach which combines FTIRI spectroscopy with histological and multivariate analyses to evaluate *ex vivo* the effects of healing abutments with conventional and experimental surfaces (i.e. machined and laser-treated) on the structural and macromolecular organization of collagen. The null hypothesis of this study is that the collagen surrounding the laser-treated surface of the healing abutment (HA) exhibits qualitative and quantitative characteristics, in terms of organization, distribution, and orientation, comparable to those observed in collagen in contact with the machined surfaces.

## Methods

### Patients' selection

N. 7 patients were selected among the thirty who participated to the first step [36]. Inclusion criteria were as follows: patients aged between 18 to 75 years; good oral and systemic health; at least 2 mm of adherent gingiva in the site chosen for rehabilitation; adequate residual bone ridge. Conversely, exclusion criteria were the following: patients with scarce oral hygiene; Full Mouth Plaque Score and Full Mouth Bleeding score greater than 25%; active periodontal disease; uncontrolled diabetes mellitus; number of cigarettes smoked per day greater than 10.

All patients, enrolled by the Implantology Operating Unit of the Department of Medical, Oral and Biotechnological Sciences, "G. d'Annunzio" University of Chieti-Pescara, signed a written informed consent to participate. The study, conducted according to the principles established in the Declaration of Helsinki (2008) developed by the World Medical Association on Humans, was approved by the Ethics Committee of the University of Chieti-Pescara "G. d'Annunzio" (18/10/2018, No. 22).

### Surgical treatment

Before surgery, patients were submitted to oral physical and radiographic examinations, such as Orthopantomography and Cone Beam Computed Tomography. The implant placement surgery was performed by an experienced surgeon (GDA) under local anesthesia obtained by infiltration of a 4% articaine solution containing

1:100,000 adrenaline. Through the preparation of a full-thickness flap, exposure of the bone ridge was achieved. The implant site was prepared by helical drills with increasing diameters to the desired measure under copious irrigation. All inserted implants (Omny, Geass srl, Pozzuoli del Friuli, Udine, Italy), had different diameters (3.50 mm, 4.1 mm) and lengths (7.0 mm, 8.0 mm, 10.0 mm, 11.5 mm). After screwing the plug screws onto the implants these were submerged. Patients were given oral hygiene instructions; antibiotic therapy (amoxicillin + clavulanic acid 2 g/day) and rinses with mouthwash with 0.20% chlorhexidine (Chlorexidine®, Oral-B, Boston, MA, USA) were prescribed for seven days. The appointment for suture removal was scheduled at 7–10 days after surgery.

The second surgical phase was performed after a healing period of  $12 \pm 4$  weeks. After uncovering the implants, the cap screws were replaced by experimental HAs, made of Grade 5 titanium (TiVaAl alloy) and with a diameter of 2.65 mm and a height of 5.08 mm (Geass srl, Pozzuoli del Friuli, Udine, Italy). The surface of these experimental HAs was subjected to two different treatments, to obtain on each HA two laser-treated (Synthegra technique) and two machined surfaces, alternating with each other (Fig. 1).

### Samples collection and preparation

After the healing period ( $30 \pm 7$  days) [40], HAs were retrieved together with the corresponding gingival biopsies collected by a 5-mm diameter circular punch. In order to have a correct orientation of the biopsies, two 7/0 sutures (OMNIA S.r.l. S. Michele Campagna Fidenza, Parma, Italy) were used to delineate the portion of gingiva in contact with one of the two laser-treated surfaces (Fig. 2).

Gingiva portions were fixed by immersion in 4% paraformaldehyde solution at 4 °C for 24 h. Then, they were washed once with 0.9% NaCl (w/w) for 5 min, twice with 70% ethanol (w/w) for 10 min, and finally stored in 70% ethanol (w/w). After dehydration with ethanol gradient [17], samples were washed with xylene (Bio-Optica, Milan, Italy), and finally detached from the healing screw and embedded in paraffin (Bio-Optica, Milan, Italy), paying attention to preserve the correct orientation and to memorize the position of the laser-treated and machined surfaces. The obtained paraffin blocks were cut according to the transverse plane (see Fig. 3) by using a microtome (Leica RM2125RTS, GmbH, Wetzlar, Germany); from each block, six 7 µm-thickness sections containing all the four alternated surfaces were obtained, and alternatively deposited onto glass slides and CaF<sub>2</sub> optical windows (13 mm diameter, 1 mm thickness), respectively for histological and FTIRI analyses.

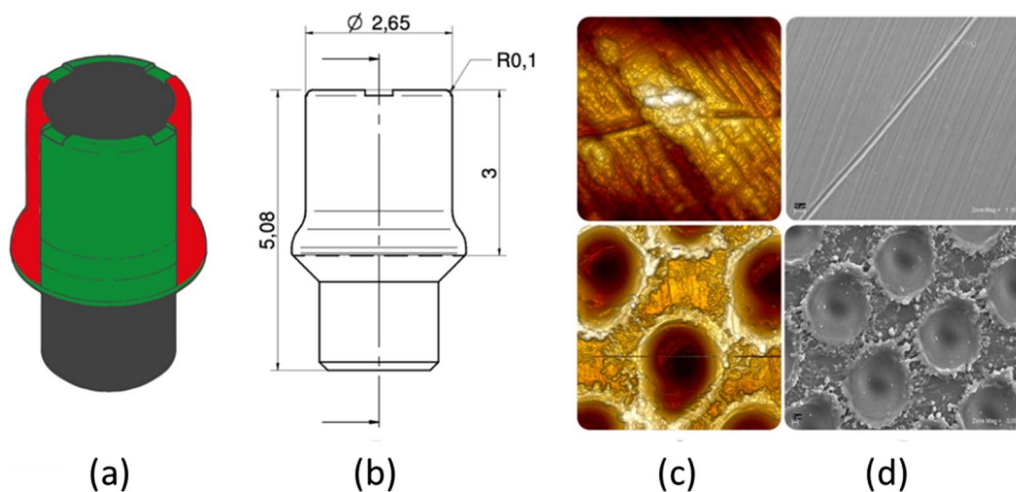


**Fig. 1** **a** Schematic description of the experimental healing abutment surface treatments (laser-treated in red and machined in green). **b** HA technical design and dimensions. **c** Atomic force microscope images of the two surface treatments (up-machined and down laser-treated). **d** Scanning electron microscope images of the machined (up) and laser-treated (down) surfaces used in the experimental HA

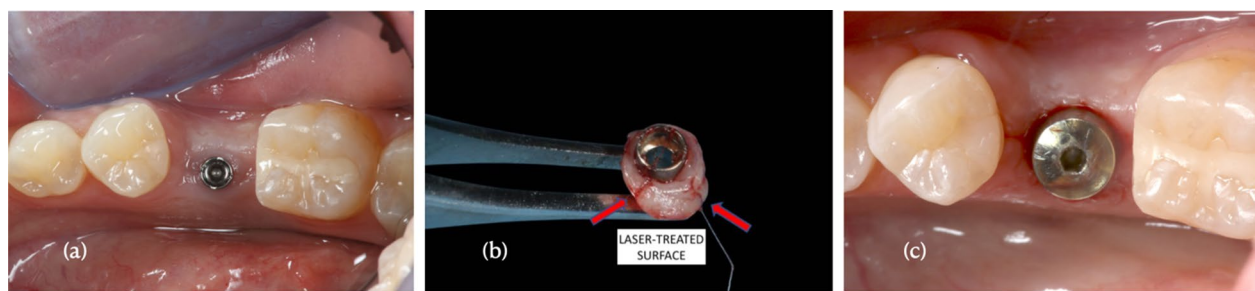


**Fig. 2** **a** Experimental HA (diameter of 2.65 mm and height of 5.08. mm). **b** Image of a representative post-operative portion of gingiva surrounding the dental implant with alternating machined and laser-treated surfaces, as indicated by the arrows. **c** The experimental healing abutments were replaced by a standard healing HA, taking care to preserve the keratinization tissue obtained during healing

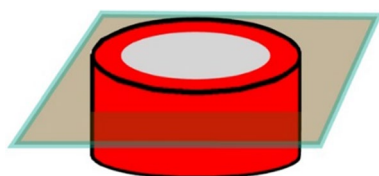


**Fig. 3** Sketch representing a paraffin block of gingival tissue (red coloured) and the transverse plane (grey square) along which the cut was made with the microtome to obtain 7 µm-thickness sections

**Histological analysis**

Seven-µm thickness sections were stained with Masson’s trichrome staining (Bio-Optica, Milan, Italy), specific for collagen which results blue coloured. The stained sections were examined by means of a Zeiss Axio Imager.A2 microscope (Zeiss, Oberkochen, Germany). The images were acquired by using the AxioCam

503 combined color digital camera (Zeiss, Oberkochen, Germany).

**FTIRI measurements**

FTIRI measurements were carried out at the Laboratory of Vibrational Spectroscopy of the Department of Life and Environmental Sciences, Polytechnic University of Marche (Ancona, Italy). A Bruker INVENIO-R interferometer coupled with a Hyperion 3000 Vis-IR microscope and equipped with a Focal Plane Array detector for tissue imaging analysis, operating at liquid nitrogen temperature (Bruker Optics, Ettlingen, Germany), was used.

The photomicrograph of each section was acquired with a 15×objective; photomicrographs were used to accurately select specific areas, corresponding to the gingival tissue close to the machined (named MACHINED) and laser-treated (named LASER) surfaces, on which acquiring IR images. The acquisition was performed

in transmission mode in the 4000–800  $\text{cm}^{-1}$  spectral range (spectral resolution 4  $\text{cm}^{-1}$ ); each IR image was  $164 \times 164 \mu\text{m}$  and consisted of 4096 pixels/spectra, with a spatial resolution for each pixel of  $2.56 \times 2.56 \mu\text{m}$ ; each pixel/spectrum was the result of 256 scans. Before proceeding with the analysis of the sample, the background spectrum was acquired on a clean region of the  $\text{CaF}_2$  optical window, using the same setup (OPUS 7.5 software package, Bruker Optics, Ettlingen, Germany). IR images were opportunely processed to avoid both the signals due to the presence of atmospheric carbon dioxide and water vapor, and artifacts caused by even slight differences in section thickness (respectively Atmospheric Compensation and Vector Normalization routines; OPUS 7.5 software package, Bruker Optics, Ettlingen, Germany).

False-color images were generated by integrating pre-processed IR images under the 1300–1185  $\text{cm}^{-1}$  region, to evaluate the spatial distribution of collagen within the mapped areas. Pre-processed IR images were also subjected to Hierarchical Cluster Analysis (HCA), using Euclidean distance and Ward's method (CytoSpec software v. 2.00.01). By comparing IR images with the relative histological ones, the clusters corresponding to collagen-rich area were identified, and the corresponding IR spectra extracted. For each patient, the mean IR spectra of each laser-treated and machined surface were calculated, together with their standard deviation spectra (Averaging routine, OPUS 7.5 software package, Bruker Optics, Ettlingen, Germany).

Mean spectra were the vector normalized and curve fitted in the 1730–1590  $\text{cm}^{-1}$  and 1360–1180  $\text{cm}^{-1}$  spectral ranges, to highlight changes in collagen secondary structure. The number and position of the underlying peaks were defined by the analysis of second derivative spectra and fixed during the curve fitting procedure; a Gaussian distribution was adopted for peak shape (GRAMS/AI 9.1,

Galactic Industries, Inc., Salem, New Hampshire). Peaks' assignment was performed in accordance with data reported in the literature [41–44]. The areas (A) of the most significant peaks were calculated and used to obtain specific spectral parameters (see “Results” section).

#### Statistical analysis

The sample size calculation was performed according to Covani et.al 2023 [45]: a sample size of 14 statistical units (surface treatment) per group was calculated to have a minimum difference of collagen fiber quantity ( $\mu\text{m}^2$ ) between the two groups. The  $\alpha$  value was determinate as 0.05 while the power of the test was 0.95. For the statistical calculation Gpower sample size software calculation was used.

Statistical analysis was performed using PRISM 6.0 software (GraphPad Software, San Diego, CA, USA). All data were presented as mean  $\pm$  SD. Statistical significance between groups was assessed using the t-test. Statistical significance was set at  $p < 0.05$  (\* $p < 0.05$ ; \*\* $p < 0.01$ ; \*\*\* $p < 0.001$  and \*\*\*\* $p < 0.0001$ ; <sup>n.s.</sup> $p > 0.05$ ).

#### Results

Representative Masson's trichrome histological images of gingival tissue adjacent to dental implants with alternated laser-treated and machined surfaces, are displayed in Fig. 3. In all the sections, a massive presence of collagen was observed, even if with a distinctive arrangement and distribution in relation with the two different implant surfaces. More in detail, a well evident longitudinal disposition is displayed by collagen bundles close to the machined surface (Fig. 4a); conversely, no specific orientation was found in collagen in the presence of the laser-treated surface, even if some bundles seem to be perpendicular to the HA (Fig. 4b).

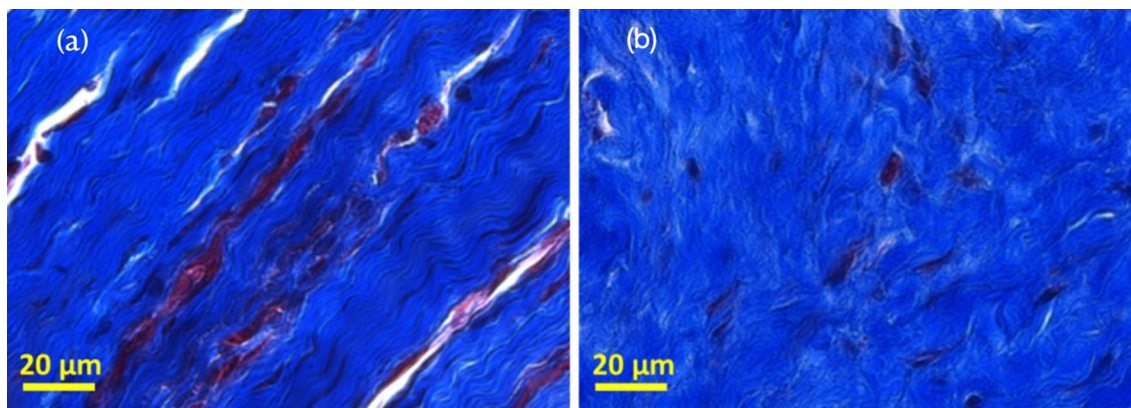
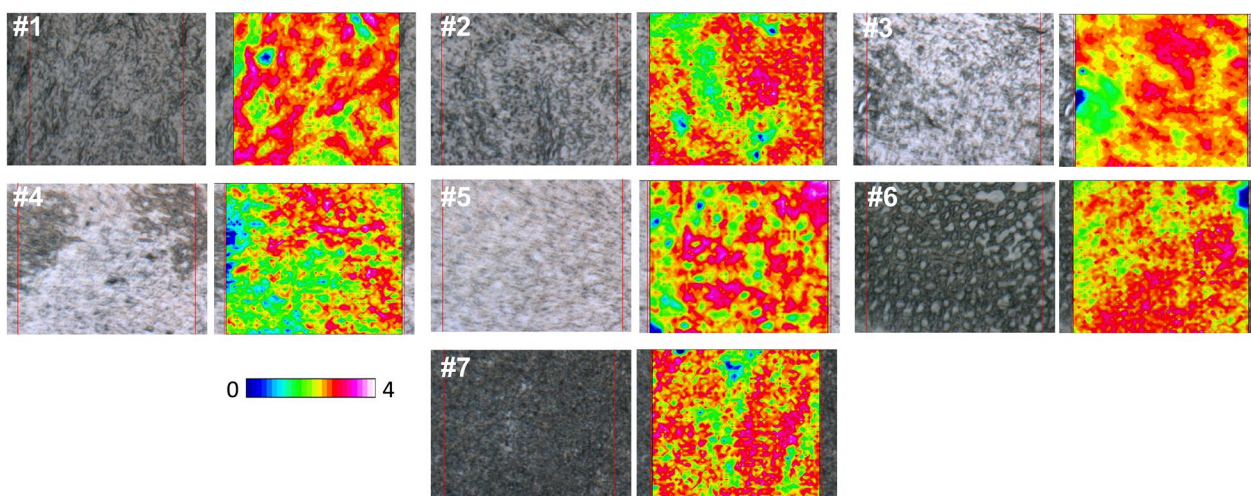


**Fig. 4** Masson's trichrome histological images of representative sections of gingival tissue adjacent to (a) machined and (b) laser-treated implant surfaces (20 $\times$  magnification)

More information on the composition and spatial distribution of collagen bundles was obtained by the hyperspectral analysis of the IR images. In Fig. 5, the photomicrographs of representative LASER and MACHINED areas for each patient (#1–#7), are reported, together with the false color images showing the spatial arrangement of the collagen bundles. False color images are a useful tool to evidence the topographical distribution of specific macromolecules, including proteins, collagen, lipids, and so on. They are generated by integrating the whole IR image under defined spectral

intervals, specific for each macromolecule. The arbitrary color scale also allows to visualize the relative quantity of the investigated macromolecule, with white/pink indicating areas with higher levels and blue/black areas with lower ones. In this study, the IR images were integrated under the  $1300\text{--}1185\text{ cm}^{-1}$  region, which includes the most diagnostic vibrational modes of collagen. Their analysis confirmed that collagen is the main component of gingival tissue, and that collagen bundles show a perpendicular orientation in the tissue adjacent to the laser-treated surface (Fig. 5b), while in the machined surface

(a) LASER



(b) MACHINED

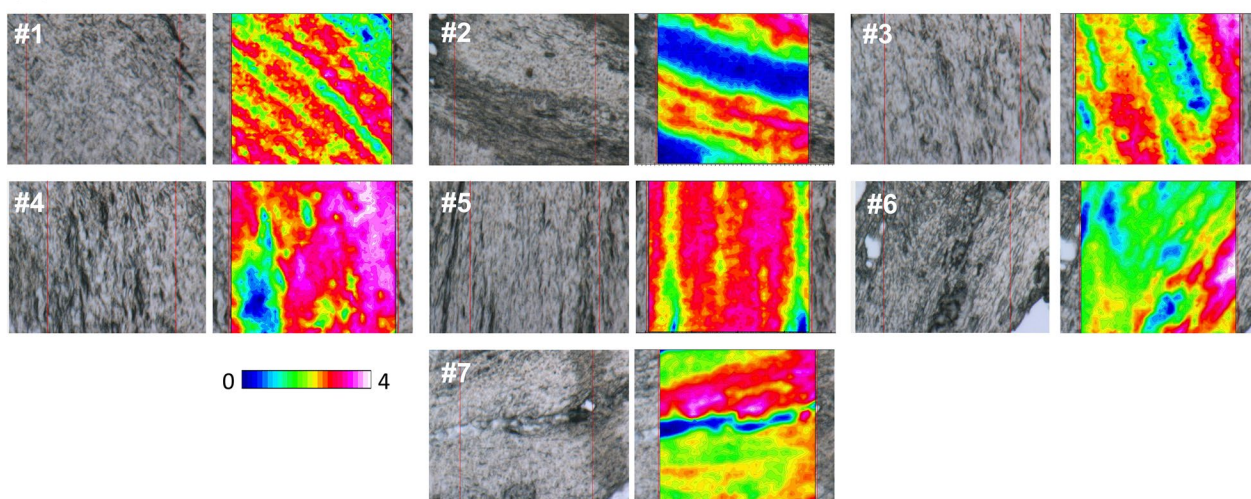


**Fig. 5** Hyperspectral analysis of the IR images collected on gingival portions adjacent to (a) laser-treated (LASER) and (b) machined (MACHINED) surfaces. For each patient (#1–#7), the photomicrographs of representative LASER and MACHINED areas are reported (on the left), together with the false color images showing the topographical distribution of collagen (on the right). The red squares in the photomicrographs indicate the areas on which IR images were collected ( $164 \times 164\ \mu\text{m}^2$ ; 4096 pixel/spectra; spatial resolution  $2.56 \times 2.56\ \mu\text{m}^2$ ). An arbitrary colored scale was adopted, white/pink colors indicating areas with the highest amount of collagen, while blue/black colors those with the lowest one

they exhibit a distribution longitudinal to the implant (Fig. 5b).

IR images were also submitted to Hierarchical Cluster Analysis (HCA), to accurately identify the areas with the highest amount of collagen, from which to extract the IR spectra. In Fig. 6a, as an example, the HCA of representative LASER and MACHINED samples is shown, different colors indicating the presence of four clusters, each characterized by a peculiar spectral profile: the clusters richer in collagen were light blue colored.

The mean absorbance IR spectra extracted from the clusters richer in collagen corresponding to LASER and MACHINED samples were analyzed in the most significant spectral ranges: 1760–1490  $\text{cm}^{-1}$  representative of total proteins (Fig. 6b), and 1360–900  $\text{cm}^{-1}$  representative of collagen (Fig. 6c). The bands centred at  $\sim 1656 \text{ cm}^{-1}$  and  $\sim 1550 \text{ cm}^{-1}$ , named respectively Amide I and II bands are related to the vibrational modes of the functional groups involved in the peptide bond (i.e. C=O, C–N and N–H) (Fig. 6b). The band at  $\sim 1340 \text{ cm}^{-1}$  is attributable to the  $\text{CH}_2$  groups in proline, the most abundant amino acid in collagen; also the bands at  $\sim 1282 \text{ cm}^{-1}$ ,  $\sim 1240 \text{ cm}^{-1}$  and  $\sim 1206 \text{ cm}^{-1}$ , named Amide III, with a typical tricuspoid shape, are mainly attributed to collagen (Fig. 6c). Finally, the bands at  $\sim 1082 \text{ cm}^{-1}$  and  $\sim 1033 \text{ cm}^{-1}$  are related respectively to phosphate groups in phosphorylated compounds and C–OH bonds in carbohydrates (Fig. 6c) [17].

Mean spectra were then curve fitted in the following spectral ranges: 1730–1590  $\text{cm}^{-1}$  and 1360–1180  $\text{cm}^{-1}$  (Fig. 7). Curve fitting is a well assessed procedure which let identify the subcomponent peaks underlying

a convoluted band. The first spectral interval (1730–1590  $\text{cm}^{-1}$ ) corresponds to the Amide I band and provides relevant and reliable information on proteins secondary structure [17, 46–48]. In particular, the bands at  $\sim 1692 \text{ cm}^{-1}$ ,  $\sim 1685 \text{ cm}^{-1}$ ,  $\sim 1630 \text{ cm}^{-1}$  and  $\sim 1621 \text{ cm}^{-1}$  are assigned to  $\beta$ -sheet structures, while those at  $\sim 1665 \text{ cm}^{-1}$  and  $\sim 1654 \text{ cm}^{-1}$  to  $\alpha$  helix ones; moreover, the bands at  $\sim 1676 \text{ cm}^{-1}$  and  $\sim 1638 \text{ cm}^{-1}$  are attributable respectively to 3-turn helix and triple helix structures; finally, the band at  $\sim 1644 \text{ cm}^{-1}$  is due to random coil structures. As regards the 1360–1180  $\text{cm}^{-1}$  range, it includes the Amide III band and is representative of the structural features of collagen [17, 49, 50]. In this spectral region, the following bands were detected:  $\sim 1342 \text{ cm}^{-1}$  (wagging of  $\text{CH}_2$  groups in proline side chains);  $\sim 1319 \text{ cm}^{-1}$  ( $\alpha$  helix structures of collagen);  $\sim 1284 \text{ cm}^{-1}$  and  $\sim 1240 \text{ cm}^{-1}$  (triple helix structures of collagen);  $\sim 1263 \text{ cm}^{-1}$  (random coil structures), and  $\sim 1202 \text{ cm}^{-1}$  (lateral chains of aminoacids) [17].

Based on curve fitting data, the following spectral parameters were calculated:  $A_{1665+1654}/A_{AI}$  (ratio between the sum of the areas of the bands at 1665  $\text{cm}^{-1}$  and 1654  $\text{cm}^{-1}$  and the area of the 1730–1590  $\text{cm}^{-1}$  range, corresponding to the Amide I band and named AI);  $A_{1644}/A_{AI}$  (ratio between the area of the band at 1644  $\text{cm}^{-1}$  and the area of the Amide I band, calculated as described above);  $A_{1638}/A_{AI}$  (ratio between the area of the band at 1638  $\text{cm}^{-1}$  and the area of the Amide I band, calculated as described above);  $A_{1342}/A_{tot}$  (ratio between the area of the band at 1342  $\text{cm}^{-1}$  and the area of the 1360–1180  $\text{cm}^{-1}$  range, named  $A_{tot}$ );  $A_{1284+1240}/A_{tot}$  (calculated as ratio between the sum of the areas of the

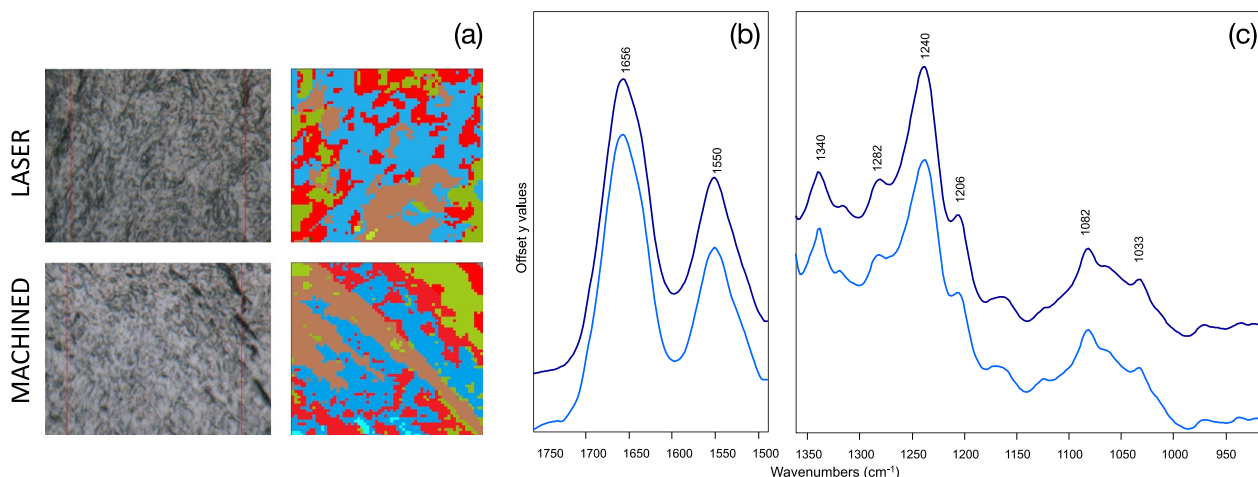


**Fig. 6** **a** Hierarchical Cluster Analysis of IR images representative of LASER and MACHINED samples (light blue color indicates the clusters richer in collagen). Mean absorbance IR spectra extracted from the clusters richer in collagen of LASER (light blue lines) and MACHINED (blue lines) samples: **b** 1760–1490  $\text{cm}^{-1}$  and **c** 1360–900  $\text{cm}^{-1}$  spectral ranges. Spectra are offset along the y axis for a better comprehension. The position of the most significant bands is indicated over the spectra (wavenumbers,  $\text{cm}^{-1}$ )

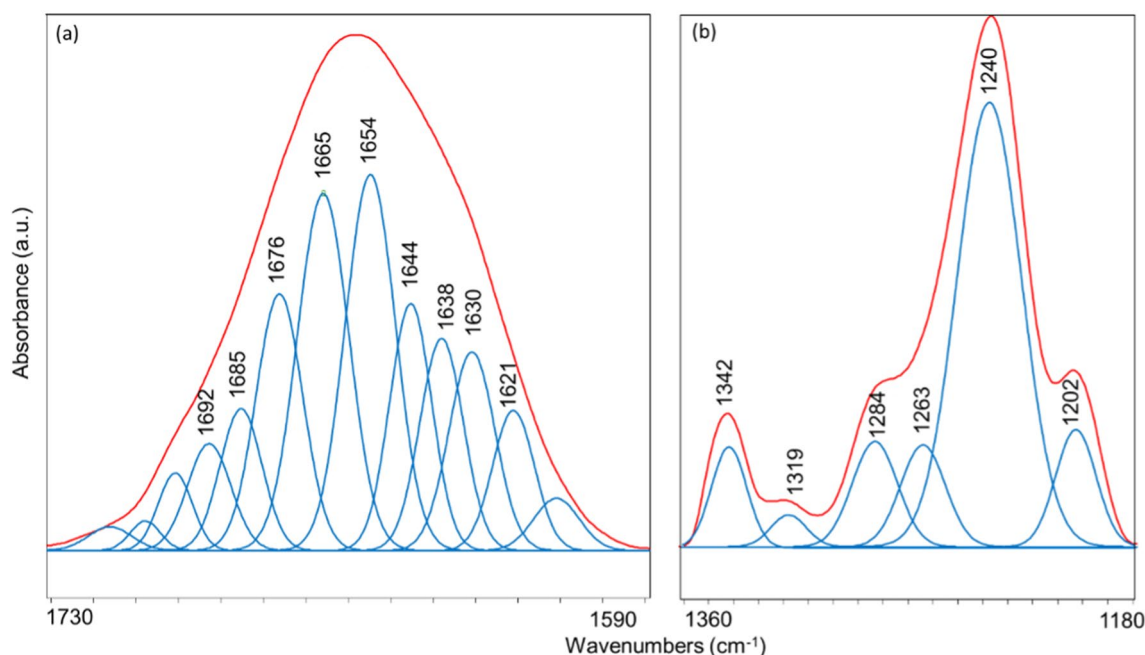


**Fig. 7** An example of curve fitting analysis performed on mean IR spectra of LASER and MACHINED samples in the (a) 1730–1590  $\text{cm}^{-1}$  and (b) 1360–1180  $\text{cm}^{-1}$  spectral ranges (the red line is the original spectrum, while blue lines indicate the subcomponent peaks, whose position is reported over peaks as wavenumbers)

bands at 1284  $\text{cm}^{-1}$  and 1240  $\text{cm}^{-1}$  and  $A_{\text{tot}}$  calculated as described above), and  $A_{1263}/A_{\text{tot}}$  (ratio between the area of the band at 1263  $\text{cm}^{-1}$  and  $A_{\text{tot}}$ , calculated as described above).

The statistical analysis of these spectral parameters is reported in Fig. 8. The ratios  $A_{1665+1654}/A_{\text{AI}}$  and  $A_{1342}/A_{\text{tot}}$  indicating, respectively the relative amount of  $\alpha$ -helix structures and proline, can be associated with the relative amount of collagen. Both show higher values in the LASER samples respect to MACHINED ones, confirming a greater quantity of collagen in the tissue near the laser-treated surface ( $A_{1665+1654}/A_{\text{AI}}$ ,  $p < 0.0001$ ;  $A_{1342}/A_{\text{tot}}$ ,  $p < 0.05$ ). The ratios  $A_{1638}/A_{\text{AI}}$  and  $A_{1284+1240}/A_{\text{tot}}$  are representative of the relative amount of triple helices, respectively in proteins and collagen, and hence they can provide information on the structural organization of collagen. Both ratios display higher values in LASER samples respect to MACHINED ones, letting hypothesize the presence of a more organized collagen in the tissue close to the laser-treated surface ( $A_{1638}/A_{\text{AI}}$ ,  $p < 0.0001$ ;  $A_{1284+1240}/A_{\text{tot}}$ ,  $p < 0.0001$ ). Finally, the ratios  $A_{1644}/A_{\text{AI}}$  and  $A_{1263}/A_{\text{tot}}$  are attributable to random coil structures, respectively in proteins and collagen. For both ratios, lower values were detected in LASER samples respect to MACHINED ones ( $A_{1644}/A_{\text{AI}}$ ,  $p < 0.0001$ ;  $A_{1263}/A_{\text{tot}}$ ,  $p < 0.0001$ ), suggesting the presence of unfolded protein structures in the latter. Hence, the higher number

of alpha and triple helices, and the lower one of random coil structures observed in LASER samples respect to MACHINED ones, let hypothesize that the laser-treated surface could promote the formation of a greater amount of collagen, with a more organized structure.

## Discussion

Over the years, new configurations and topographic characterizations have been proposed and investigated to improve the soft tissue attachment to the transmucosal part of dental implants [51–53]. A satisfactory bone-to-implant connection could not alone guarantee a long-term success of dental implants [3, 54]. Indeed, the clinical success is also related to the quality of soft tissues surrounding the implant neck and to the orientation of the peri-implant collagen fibers [55]. After implant insertion, gingival fibroblasts begin to proliferate, repopulate, and generate a collagen-rich extracellular matrix in the transmucosal region that adheres to the HA [56, 57]. This physical barrier between the oral cavity and the osseous support of the implant, is represented by collagen fibers, whose well-organization were hypothesized to decrease early bone resorption by reducing bacteria infiltration, due to the formation of a soft tissue barrier [5, 6, 58]. For this reason, the surface characteristics of the HA play an important role in a strategic area of deep tissue remodeling, by creating

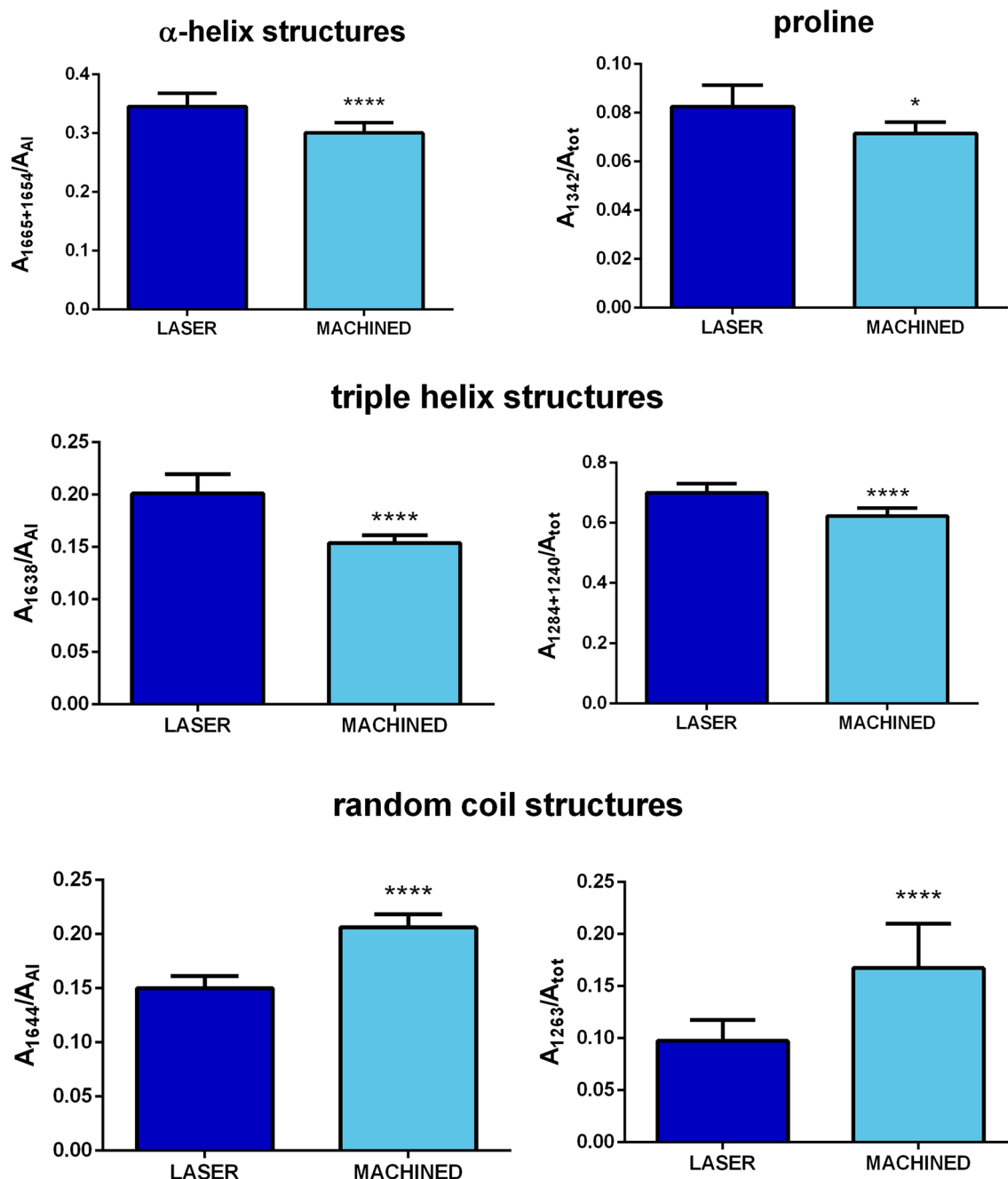


**Fig. 8** Statistical analysis (t-test) of proteins and collagen secondary structure in gingival portions adjacent to laser-treated (LASER) and machined (MACHINED) surfaces: α-helix structures ( $A_{1665+1654}/A_{AI}$ ), proline ( $A_{1342}/A_{tot}$ ), triple helix structures ( $A_{1638}/A_{AI}$  and  $A_{1284+1240}/A_{tot}$ ), and random coil structures ( $A_{1644}/A_{AI}$  and  $A_{1263}/A_{tot}$ ). Data are shown as mean ± SD; asterisks over histograms indicate statistically significant differences (\*p < 0.05; \*\*p < 0.01; \*\*\*p < 0.001 and \*\*\*\*p < 0.0001)

a biologic width and influencing collagen fiber orientation [59, 60]. Until now, in implantology, the scientific literature has not clarified whether it is preferable to have a transgingival implant portion with controlled roughness or a machined one [61]. According to some authors, the transgingival portion with a machined

surface may reduce the adhesion of bacteria and the consequent risk of bacterial colonization and inflammation of soft and hard tissues around dental implant [62, 63]. From this perspective, a machined implant collar could reduce the occurrence of peri-implantitis [64]. At this purpose, in this study, the machined surface of

HA was considered as control and compared with the laser-treated, considered the experimental surface [65].

The results of the present study support the rejection of the null hypothesis. Indeed, in all the analyzed cross-sections, the histological analysis evidenced a massive presence of collagen in the tissue around the HA, with a surface-related spatial pattern: a well evident longitudinal disposition is displayed by collagen bundles close to the machined surface, while in the presence of the laser-treated surface, collagen does not show a specific orientation, even the majority of the bundles seem to be perpendicular to the HA. These differences were better highlighted by the analysis of the IR images, which confirmed that collagen is the main component of all the analyzed samples, and that bundles exhibited a longitudinal distribution to the implant in the machined surface, whereas in the tissue adjacent to the laser-treated one, the fibers are randomly distributed, with a prevalence of perpendicular orientation. It is well known that while moderate crosslinking positively impacts collagen fiber mechanical properties, excessive crosslinking renders these fibers more fragile [66]. Moreover, several authors have suggested in human and animal histologic studies that collagen circular orientation around HA could not stabilize the peri-implant connective tissues [67, 68]. Indeed, the fibers aligned in a parallel orientation around dental implants could be considered not functional, whereas the functional physical orientation is represented by a perpendicular pattern [69, 70]. This kind of attachment is similar to that of a natural tooth, which is an indispensable barrier against bacterial infection and other harmful stimuli.

It is, also, known that transmucosal connective tissue integration is achieved by a small number of gingival fibroblasts (only 3–5%) in mature peri-implant connective tissue, which is significantly lower than the concentration of gingival fibroblasts in healthy periodontal connective tissue (approximately 15%) [71]. The lack of fiber connection to the abutment surface and the lower amount of gingival fibroblasts produce a poorly integrated transmucosal connective tissue layer on the dental implant abutments. The enhancement of fibroblast functions can be reached through appropriate topographical/biological modifications of the abutment faces [32, 72]. Our previously human clinical studies evaluated the biological advantages of using transmucosal components with a rough surface characterized by a controlled topography formed by micrometric regular pores. This kind of surface, obtained with the Synthebra technique, have demonstrated a positive influence on cell adhesion [36] and a reduced inflammatory infiltrate [35], suggesting a good chance of positively influencing the difficult coronal biological seal formation. The present results are in

line with the previously published one and enhance the importance of surface treatment on the biological structural organization of the peri-implant soft tissues.

In this study, a higher amount of collagen was found in the laser-treated surface ( $A_{1342}/A_{tot}$  and  $A_{1665+1654}/A_{AI}$  band area ratios, relative, respectively to proline and  $\alpha$ -helices). Evidence of a different secondary structure was also highlighted by the univariate analysis of specific band area ratios. In particular, collagen close to the laser-treated surface is characterized by the presence of a major number of triple helices ( $A_{1638}/A_{AI}$  band area ratio) and less random coil structures ( $A_{1644}/A_{AI}$ ,  $p < 0.01$  band area ratio), letting hypothesize that this collagen is more similar to the native one [42].

A limitation of the current study may be the short follow-up ( $12 \pm 4$  weeks) which does not allow to compare the intensity of the cellular events in peri-implant tissues after implant loading. However, it is reported that the peri-implant soft tissue clinical maturity is established 4 weeks following implant placement by a one-stage surgical protocol [73].

Thus, our findings, supported by previous literature, suggest that during extracellular matrix maturation around the HA, the local microenvironment could be influenced by the different HA surface treatments and that the collagen orientation near the laser-treated surfaces could allow a better preservation of the peri-implant bone resorption.

However, further studies are necessary to better understand and characterize the gingival tissues around HA, focusing on the peri-implant connective fibers orientations.

## Conclusions

The results of this study demonstrate how the use of a laser-treated transmucosal surface can improve the morphological organization of peri-implant soft tissue. In fact, the collagen tissue formed around the surface of the laser-treated abutment, in addition to being present in greater quantity, also displayed a more organized distribution with a higher amount of triple helices, respect to the collagen near the machined one. This finding let hypothesize a good degree of maturation, similar to that found in natural teeth.

Even if all these findings suggest that the laser-treated surface can promote the formation of a soft tissue able to provide a better seal, further studies will be needed to fully understand the role of such a topography-controlled surface for improving this sealing and increasing the performance and longevity of dental implants.

## Abbreviations

HA Healing abutments

FTIRI Fourier Transform InfraRed Imaging  
HCA Hierarchical cluster analysis

#### Author contributions

Conceptualization, BS, SC and GO; methodology, GORI, AB and GA; software, EG, AB and VN; validation, EG, BS and SC; formal analysis, VN, GORI, EG and GO; investigation, GA, GDA; resources, SC, EG and GO; data curation, AB, GORI, VR and EG; writing—original draft preparation, AB, GA, VR and GORI; writing—review and editing, BS, GDA, EG and GO; supervision, SC, GO, EG and BS; project administration, BS, GO and EG; funding acquisition, GO, SC and BS. All authors have read and agreed to the published version of the manuscript.

#### Funding

This work was partially supported by a grant from the Italian Ministry of University and Research (MIUR) ('PRIN' 2022, project Prot. 2022MKE4AF).

#### Availability of data and materials

The datasets used and/or analyzed during the current study are available after request to the corresponding author.

#### Declarations

#### Ethics approval and consent to participate

The study was approved by the Ethical Committee of "G.d'Annunzio" Chieti-Pescara University. On October 18, 2018, number 22. Patients gave written informed consent and received information about the study protocol. The study was conducted in accordance with the principles of the Helsinki Declaration established by the World Medical Association regarding human subjects.

#### Consent for publication

Not applicable.

#### Competing interests

The authors declare that they have no competing interest.

#### Author details

<sup>1</sup>Department of Life and Environmental Sciences, Polytechnic University of Marche, Ancona, Italy. <sup>2</sup>Electron Microscopy Laboratory, Department of Innovative Technologies in Medicine and Dentistry, University "G. d'Annunzio" Chieti-Pescara, Chieti, Italy. <sup>3</sup>Department of Clinical Sciences and Stomatology, Polytechnic University of Marche, Ancona, Italy.

Received: 23 June 2023 Accepted: 18 January 2024

Published online: 31 January 2024

#### References

- Albrektsson T, Zarb G, Worthington P, Eriksson AR. The long-term efficacy of currently used dental implants: a review and proposed criteria of success. *Int J Oral Maxillofac Implants*. 1986;1:11–25.
- Do TA, Le HS, Shen Y-W, Huang H-L, Fuh L-J. Risk factors related to late failure of dental implant—a systematic review of recent studies. *Int J Environ Res Public Health*. 2020;17:3931. <https://doi.org/10.3390/ijerph17113931>.
- Esposito M, Hirsch JM, Lekholm U, Thomsen P. Biological factors contributing to failures of osseointegrated oral implants. (I). Success criteria and epidemiology. *Eur J Oral Sci*. 1998;106:527–51. <https://doi.org/10.1046/j.0909-8836.t01-2-.x>.
- Tonetti MS, Schmid J. Pathogenesis of implant failures. *Periodontol*. 1994;2000(4):127–38. <https://doi.org/10.1111/j.1600-0757.1994.tb00013.x>.
- Ericsson I, Berglundh T, Marinello C, Liljenberg B, Lindhe J. Long-standing plaque and gingivitis at implants and teeth in the dog. *Clin Oral Implants Res*. 1992;3:99–103. <https://doi.org/10.1034/j.1600-0501.1992.030301.x>.
- Lang N, Berglundh T, Lang NP, Berglundh T. Working Group 4 of Seventh European Workshop on Periodontology. Peri-implant diseases: Where are we now?—Consensus of the Seventh European Workshop on Periodontology. *J Clin Periodontol*. 2011;38(Suppl 11):178–81. <https://doi.org/10.1111/j.1600-051X.2010.01674.x>.
- Pontoriero R, Tonelli MP, Carnevale G, Mombelli A, Nyman SR, Lang NP. Experimentally induced peri-implant mucositis. A clinical study in humans. *Clin Oral Implants Res*. 1994;5:254–9.
- Roos-Jansåker A-M, Renvert H, Lindahl C, Renvert S. Nine- to fourteen-year follow-up of implant treatment. Part III: factors associated with peri-implant lesions. *J Clin Periodontol*. 2006;33:296–301. <https://doi.org/10.1111/j.1600-051X.2006.00908.x>.
- Quiryneen M, De Soete M, van Steenberghe D. Infectious risks for oral implants: a review of the literature. *Clin Oral Implants Res*. 2002;13:1–19. <https://doi.org/10.1034/j.1600-0501.2002.130101.x>.
- Mombelli A. In vitro models of biological responses to implant microbiological models. *Adv Dent Res*. 1999;13:67–72. <https://doi.org/10.1177/08959374990130011701>.
- Berglundh T, Lindhe J, Marinello C, Ericsson I, Liljenberg B. Soft tissue reaction to de novo plaque formation on implants and teeth. An experimental study in the dog. *Clin Oral Implants Res*. 1992;3:1–8. <https://doi.org/10.1034/j.1600-0501.1992.030101.x>.
- Lindhe J, Berglundh T, Ericsson I, Liljenberg B, Marinello C. Experimental breakdown of peri-implant and periodontal tissues. A study in the beagle dog. *Clin Oral Implants Res*. 1992;3:9–16. <https://doi.org/10.1034/j.1600-0501.1992.030102.x>.
- Tete S, Mastrangelo F, Bianchi A, Zizzari V, Scarano A. Collagen fiber orientation around machined titanium and zirconia dental implant necks: an animal study. *Int J Oral Maxillofac Implants*. 2009;24:52–8.
- Querido W, Kandel S, Pleshko N. Applications of vibrational spectroscopy for analysis of connective tissues. *Molecules*. 2021;26:922. <https://doi.org/10.3390/molecules26040922>.
- Frantz C, Stewart KM, Weaver VM. The extracellular matrix at a glance. *J Cell Sci*. 2010;123:4195–200. <https://doi.org/10.1242/jcs.023820>.
- Leppert PC, Baginski T, Prupas C, Catherino WH, Pletcher S, Segars JH. Comparative ultrastructure of collagen fibrils in uterine leiomyomas and normal myometrium. *Fertil Steril*. 2004;82:1182–7. <https://doi.org/10.1016/j.fertnstert.2004.04.030>.
- Belloni A, Furlani M, Greco S, Notarstefano V, Pro C, Randazzo B, Pellegrino P, Zannotti A, Carpini GD, Ciavattini A, Di Lillo F, Giorgini E, Giuliani A, Cinti S, Ciarmela P. Uterine leiomyoma as useful model to unveil morphometric and macromolecular collagen state and impairment in fibrotic diseases: an ex-vivo human study. *Biochim Biophys Acta Mol Basis Dis*. 2022;1868:166494. <https://doi.org/10.1016/j.bbdis.2022.166494>.
- Gargiulo AW, Wentz FM, Orban B. Dimensions and relations of the denotogingival junction in humans. *J Periodontol*. 1961;32:261–7. <https://doi.org/10.1902/jop.1961.32.3.261>.
- Watts T. Clinical periodontology and implant dentistry, 4th edition. *Br Dent J*. 2003;195:722–722. <https://doi.org/10.1038/sj.bdj.4810851>.
- Berglundh T, Lindhe J. Dimension of the periimplant mucosa. Biological width revisited. *J Clin Periodontol*. 1996;23:971–3.
- Chavrier C, Couble ML, Hartmann DJ. Qualitative study of collagenous and noncollagenous glycoproteins of the human healthy keratinized mucosa surrounding implants. *Clin Oral Implants Res*. 1994;5:17–24. <https://doi.org/10.1034/j.1600-0501.1994.050301.x>.
- Schwarz F, Derks J, Monje A, Wang H-L. Peri-implantitis. *J Periodontol*. 2018;89(Suppl 1):S267–90. <https://doi.org/10.1002/JPER.16-0350>.
- Ericsson I, Lindhe J. Probing depth at implants and teeth. An experimental study in the dog. *J Clin Periodontol*. 1993;20:623–7. <https://doi.org/10.1111/j.1600-051x.1993.tb00706.x>.
- Fujii N, Kusakari H, Maeda T. A histological study on tissue responses to titanium implantation in rat maxilla: the process of epithelial regeneration and bone reaction. *J Periodontol*. 1998;69:485–95. <https://doi.org/10.1902/jop.1998.69.4.485>.
- Iglhaut G, Schwarz F, Winter RR, Mihatic I, Stimmelmayer M, Schliephake H. Epithelial attachment and downgrowth on dental implant abutments—a comprehensive review. *J Esthet Restor Dent*. 2014;26:324–31. <https://doi.org/10.1111/jerd.12097>.
- Gittens RA, Scheideler L, Rupp F, Hyzy SL, Geis-Gerstorf J, Schwartz Z, Boyan BD. A review on the wettability of dental implant surfaces II: biological and clinical aspects. *Acta Biomater*. 2014;10:2907–18. <https://doi.org/10.1016/j.actbio.2014.03.032>.
- Ma Q, Wang W, Chu PK, Mei S, Ji K, Jin L, Zhang Y. Concentration- and time-dependent response of human gingival fibroblasts to fibroblast growth factor 2 immobilized on titanium dental implants. *Int J Nanomed*. 2012;7:1965–76. <https://doi.org/10.2147/IJN.S29538>.

28. Sugawara S, Maeno M, Lee C, Nagai S, Kim DM, Da Silva J, Nagai M, Kondo H. Establishment of epithelial attachment on titanium surface coated with platelet activating peptide. *PLoS ONE*. 2016;11:e0164693. <https://doi.org/10.1371/journal.pone.0164693>.
29. van Dijk IA, Beker AF, Jellema W, Nazmi K, Wu G, Wismeijer D, Krawczyk PM, Bolscher JGM, Veerman ECI, Stap J. Histatin 1 enhances cell adhesion to titanium in an implant integration model. *J Dent Res*. 2017;96:430–6. <https://doi.org/10.1177/0022034516681761>.
30. Di Baldassarre A, Cimetta E, Bollini S, Gaggi G, Ghinassi B. Human-induced pluripotent stem cell technology and cardiomyocyte generation: progress and clinical applications. *Cells*. 2018;7:48. <https://doi.org/10.3390/cells7060048>.
31. Mangano C, Mangano FG, Shibli JA, Roth LA, D'Addazio G, Piattelli A, Iezzi G. Immunohistochemical evaluation of peri-implant soft tissues around machined and direct metal laser sintered (DMLS) healing abutments in humans. *Int J Environ Res Public Health*. 2018;15:1611. <https://doi.org/10.3390/ijerph15081611>.
32. Bächle M, Kohal RJ. A systematic review of the influence of different titanium surfaces on proliferation, differentiation and protein synthesis of osteoblast-like MG63 cells. *Clin Oral Implants Res*. 2004;15:683–92. <https://doi.org/10.1111/j.1600-0501.2004.01054.x>.
33. Di Giulio M, Traini T, Sinjari B, Nostro A, Caputi S, Cellini L. *Porphyromonas gingivalis* biofilm formation in different titanium surfaces, an in vitro study. *Clin Oral Implants Res*. 2016;27:918–25. <https://doi.org/10.1111/clr.12659>.
34. Sinjari B, Guarnieri S, Diomedea F, Merciaro I, Mariggio MA, Caputi S, Trubiani O. Influence of titanium laser surface geometry on proliferation and on morphological features of human mandibular primary osteoblasts. *J Biol Regul Homeost Agents*. 2012;26:505–13.
35. Ghinassi B, Di Baldassarre A, D'Addazio G, Traini T, Andrisani M, Di Vincenzo G, Gaggi G, Piattelli M, Caputi S, Sinjari B. Gingival response to dental implant: comparison study on the effects of new nanopored laser-treated vs. traditional healing abutments. *Int J Mol Sci*. 2020;21:6056. <https://doi.org/10.3390/ijms21176056>.
36. Ghinassi B, D'Addazio G, Di Baldassarre A, Femminella B, Di Vincenzo G, Piattelli M, Gaggi G, Sinjari B. Immunohistochemical results of soft tissues around a new implant healing-abutment surface: a human study. *J Clin Med*. 2020;9:1009. <https://doi.org/10.3390/jcm9041009>.
37. Paraskevaidi M, Matthew BJ, Holly BJ, Hugh BJ, Thulya CPV, Loren C, StJohn C, Peter G, Callum G, Sergei KG, Kamila K, Maria K, Kássio LMG, Pierre M-HL, Evangelos P, Savithri P, John AA, Alexandra S, Marfran S, Josep S-S, Gunjan T, Michael W, Bayden W. Clinical applications of infrared and Raman spectroscopy in the fields of cancer and infectious diseases. *Appl Spectrosc Rev*. 2021;56:804–68. <https://doi.org/10.1080/05704928.2021.1946076>.
38. Belloni A, Montanari E, Sagrati A, Lorenzi T, Balloni A, Busardò FP, Notarstefano V, Fabri M, Giorgini E. Novel insights from Fourier-transform infrared imaging on the morpho-chemical profile of human corpus callosum. *Appl Sci*. 2023;13:3954. <https://doi.org/10.3390/app13063954>.
39. Licini C, Notarstefano V, Marchi S, Cerqueni G, Ciapetti G, Vitale-Brovarone C, Giorgini E, Mattioli-Belmonte M. Altered type I collagen networking in osteoporotic human femoral head revealed by histomorphometric and Fourier transform infrared imaging correlated analyses. *BioFactors Oxf Engl*. 2022;48:1089–110. <https://doi.org/10.1002/biof.1870>.
40. Femminella B, Iaconi MC, Di Tullio M, Romano L, Sinjari B, D'Arcangelo C, De Ninis P, Paolantonio M. Clinical comparison of platelet-rich fibrin and a gelatin sponge in the management of palatal wounds after epithelialized free gingival graft harvest: a randomized clinical trial. *J Periodontol*. 2016;87:103–13. <https://doi.org/10.1902/jop.2015.150198>.
41. Balan V, Mihai C-T, Cojocaru F-D, Uritu C-M, Dodi G, Botezat D, Gardikiotis I. Vibrational spectroscopy fingerprinting in medicine: from molecular to clinical practice. *Materials*. 2019;12:2884. <https://doi.org/10.3390/ma12182884>.
42. Belbachir K, Noreen R, Gouspillou G, Petibois C. Collagen types analysis and differentiation by FTIR spectroscopy. *Anal Bioanal Chem*. 2009;395:829–37. <https://doi.org/10.1007/s00216-009-3019-y>.
43. Barnas E, Skret-Magierlo J, Skret A, Kaznowska E, Depciuch J, Szmuc K, Łach K, Krawczyk-Marc I, Cebulski J. Simultaneous FTIR and Raman spectroscopy in endometrial atypical hyperplasia and cancer. *Int J Mol Sci*. 2020;21:4828. <https://doi.org/10.3390/ijms21144828>.
44. Stani C, Vaccari L, Mitri E, Birarda G. FTIR investigation of the secondary structure of type I collagen: new insight into the amide III band. *Spectrochim Acta A Mol Biomol Spectrosc*. 2020;229:118006. <https://doi.org/10.1016/j.saa.2019.118006>.
45. Covani U, Giammarinaro E, Di Pietro N, Boncompagni S, Rastelli G, Romasco T, Velasco-Ortega E, Jimenez-Guerra A, Iezzi G, Piattelli A, Marcocncini S. Electron microscopy (EM) analysis of collagen fibers in the peri-implant soft tissues around two different abutments. *J Funct Biomater*. 2023;14:445. <https://doi.org/10.3390/jfb14090445>.
46. Noreen R, Moenner M, Hwu Y, Petibois C. FTIR spectro-imaging of collagens for characterization and grading of gliomas. *Biotechnol Adv*. 2012;30:1432–46. <https://doi.org/10.1016/j.biotechadv.2012.03.009>.
47. Talari ACS, Martinez MAG, Movasaghi Z, Rehman S, Rehman IU. Advances in Fourier transform infrared (FTIR) spectroscopy of biological tissues. *Appl Spectrosc Rev*. 2017;52:456–506. <https://doi.org/10.1080/05704928.2016.1230863>.
48. Byler DM, Susi H. Examination of the secondary structure of proteins by deconvoluted FTIR spectra. *Biopolymers*. 1986;25:469–87. <https://doi.org/10.1002/bip.360250307>.
49. Cai S, Singh BR. Identification of beta-turn and random coil amide III infrared bands for secondary structure estimation of proteins. *Biophys Chem*. 1999;80:7–20. [https://doi.org/10.1016/s0301-4622\(99\)00060-5](https://doi.org/10.1016/s0301-4622(99)00060-5).
50. Singh BR, DeOliveira D, Fu F-N, Fuller M. Fourier transform infrared analysis of amide III bands of proteins for the secondary structure estimation, SPIE 1890 (1993). <https://doi.org/10.1117/12.145242>.
51. Comut AA, Weber HP, Shortkroff S, Cui FZ, Spector M. Connective tissue orientation around dental implants in a canine model. *Clin Oral Implants Res*. 2001;12:433–40. <https://doi.org/10.1034/j.1600-0501.2001.120502.x>.
52. Notthdurft FP, Fontana D, Ruppenthal S, May A, Aktas C, Mehraein Y, Lipp P, Kaestner L. Differential behavior of fibroblasts and epithelial cells on structured implant abutment materials: a comparison of materials and surface topographies. *Clin Implant Dent Relat Res*. 2015;17:1237–49. <https://doi.org/10.1111/cid.12253>.
53. Guarnieri R, Miccoli G, Reda R, Mazzoni A, Di Nardo D, Testarelli L. Laser microgrooved vs. machined healing abutment disconnection/reconnection: a comparative clinical, radiographical and biochemical study with split-mouth design. *Int J Implant Dent*. 2021;7:19. <https://doi.org/10.1186/s40729-021-00301-6>.
54. Gulati K, Moon H-J, Kumar PTS, Han P, Ivanovski S. Anodized anisotropic titanium surfaces for enhanced guidance of gingival fibroblasts. *Mater Sci Eng C Mater Biol Appl*. 2020;112:110860. <https://doi.org/10.1016/j.msec.2020.110860>.
55. Myshin HL, Wiens JP. Factors affecting soft tissue around dental implants: a review of the literature. *J Prosthet Dent*. 2005;94:440–4. <https://doi.org/10.1016/j.prosdent.2005.08.021>.
56. Stern IB. Current concepts of the dentogingival junction: the epithelial and connective tissue attachments to the tooth. *J Periodontol*. 1981;52:465–76. <https://doi.org/10.1902/jop.1981.52.9.465>.
57. Linden GJ, Mullally BH, Freeman R. Stress and the progression of periodontal disease. *J Clin Periodontol*. 1996;23:675–80. <https://doi.org/10.1111/j.1600-051x.1996.tb00593.x>.
58. Lindhe J, Meyle J, on behalf of G.D. of the E.W. on Periodontology. Peri-implant diseases: consensus Report of the Sixth European Workshop on Periodontology. *J Clin Periodontol*. 2008;35:282–5. <https://doi.org/10.1111/j.1600-051X.2008.01283.x>.
59. Ivanovski S, Lee R. Comparison of peri-implant and periodontal marginal soft tissues in health and disease. *Periodontol*. 2018;2000(76):116–30. <https://doi.org/10.1111/prd.12150>.
60. Heitz-Mayfield LJA, Lang NP. Comparative biology of chronic and aggressive periodontitis vs. peri-implantitis. *Periodontol*. 2010;53:167–81. <https://doi.org/10.1111/j.1600-0757.2010.00348.x>.
61. Chai WL, Moharamzadeh K, Brook IM, Van Noort R. A review of histomorphometric analysis techniques for assessing implant-soft tissue interface. *Biotech Histochem*. 2011;86:242–54. <https://doi.org/10.3109/10520291003707916>.
62. Abrahamsson I, Zitzmann NU, Berglundh T, Linder E, Wennerberg A, Lindhe J. The mucosal attachment to titanium implants with different surface characteristics: an experimental study in dogs. *J Clin Periodontol*. 2002;29:448–55. <https://doi.org/10.1034/j.1600-051x.2002.290510.x>.
63. Kloss FR, Steinmüller-Nethl D, Stigler RG, Ennemoser T, Rasse M, Hächli O. In vivo investigation on connective tissue healing to polished surfaces

- with different surface wettability. *Clin Oral Implants Res.* 2011;22:699–705. <https://doi.org/10.1111/j.1600-0501.2010.02038.x>.
64. Albrektsson T, Canullo L, Cochran D, De Bruyn H. "Peri-Implantitis": a complication of a foreign body or a man-made "disease". Facts and fiction. *Clin Implant Dent Relat Res.* 2016;18:840–9. <https://doi.org/10.1111/cid.12427>.
  65. Corvino E, Pesce P, Mura R, Marcano E, Canullo L. Influence of modified titanium abutment surface on peri-implant soft tissue behavior: a systematic review of in vitro studies. *Int J Oral Maxillofac Implants.* 2020;35:503–19. <https://doi.org/10.11607/jomi.8110>.
  66. Buehler MJ. Nature designs tough collagen: explaining the nanostructure of collagen fibrils. *Proc Natl Acad Sci USA.* 2006;103:12285–90. <https://doi.org/10.1073/pnas.0603216103>.
  67. Schierano G, Ramieri G, Cortese M, Aimetti M, Preti G. Organization of the connective tissue barrier around long-term loaded implant abutments in man. *Clin Oral Implants Res.* 2002;13:460–4. <https://doi.org/10.1034/j.1600-0501.2002.130503.x>.
  68. Ruggeri A, Franchi M, Marini N, Trisi P, Piatelli A. Supracrestal circular collagen fiber network around osseointegrated nonsubmerged titanium implants. *Clin Oral Implants Res.* 1992;3:169–75. <https://doi.org/10.1034/j.1600-0501.1992.030403.x>.
  69. Nevins M, Nevins ML, Camelo M, Boyesen JL, Kim DM. Human histologic evidence of a connective tissue attachment to a dental implant. *Int J Periodontics Restorative Dent.* 2008;28:111–21.
  70. Geurs NC, Vassilopoulos PJ, Reddy MS. Histologic evidence of connective tissue integration on laser microgrooved abutments in humans. *Clin Adv Periodontics.* 2011;1:29–33. <https://doi.org/10.1902/cap.2011.100005>.
  71. Liu M, Zhou J, Yang Y, Zheng M, Yang J, Tan J. Surface modification of zirconia with polydopamine to enhance fibroblast response and decrease bacterial activity in vitro: a potential technique for soft tissue engineering applications. *Colloids Surf B Biointerfaces.* 2015;136:74–83. <https://doi.org/10.1016/j.colsurfb.2015.06.047>.
  72. Lindhe J, Berglundh T. The interface between the mucosa and the implant. *Periodontol.* 1998;2000(17):47–54. <https://doi.org/10.1111/j.1600-0757.1998.tb00122.x>.
  73. DeAngelo SJ, Kumar PS, Beck FM, Tatakis DN, Leblebicioglu B. Early soft tissue healing around one-stage dental implants: clinical and microbiologic parameters. *J Periodontol.* 2007;78:1878–86. <https://doi.org/10.1902/jop.2007.070122>.

## Publisher's Note

Springer Nature remains neutral with regard to jurisdictional claims in published maps and institutional affiliations.